Linear augmented cylindrical wave method for calculating the electronic structure of double-wall carbon nanotubes

P. N. D'yachkov and D. V. Makaev*

Institute of General and Inorganic Chemistry, Russian Academy of Sciences, Leninskii pr. 31, 119991 Moscow, Russia

Electronic structure of double-wall carbon nanotubes (DWNTs) consisting of two concentric graphene cylinders with extremely strong covalent bonding of atoms within the individual graphitic sheets, but very weak van der Waals type interaction between them is calculated in the terms of the linear augmented cylindrical wave (LACW) method. A one-electron potential is used and the approximations are made in the sense of muffin-tin (MT) potentials and local density functional theory only. The atoms of DWNT are considered to be enclosed between cylinder-shaped potential barriers. In this approach, the electronic spectrum of the DWNTs is governed by the free movement of electron in the interatomic space of two cylindrical layers, by electron scattering on the MT spheres, and by electron tunneling between the layers. We have calculated the complete band structures and densities of states in the Fermi level region of the purely semiconducting zigzag DWNTs $(n,0)@(n',0)$ ($10 \leq n \leq 23$ and $19 \leq n' \leq 32$) with interlayer distance 3.2 Å $\leq \Delta d \leq$ 3.7 Å. Analogously data are obtained for metallic armchair $(n,n)@(n',n')$ nanotubes ($n=5$ or 4 and $n'=10$ or 9). According to the LACW calculations, the interwall coupling results in a distinctly stronger perturbation of the band structure of inner tube as compared to that of the outer one. In the case of semiconducting DWNTs, the minimum gap E_{11} between the singularities of the conduction and valence bands of the shell tubules decreases from 0.15 to 0.22 eV or increases from 0.7 to 0.15 eV, if dividing n' by three leaves a remainder of 1 or 2, respectively. In both cases, the ΔE_{11} shifts of the gap do not decay, but slightly oscillate as one goes to the tubules with larger diameters d. For inner tubules, the ΔE_{11} shift depends strongly on the d. For $n \bmod 3 = 2$ series with $10 \leq n \leq 16$, the shifts ΔE_{11} are positive, the maximum values of ΔE_{11} being equal to 0.39 and 0.32 eV, respectively. As one goes to the inner tubules with larger diameters, the shift ΔE_{11} quickly decays and thereupon varies between 0.06 and −0.05 eV. In the case of armchair DWNTs, the interlayer coupling does not break down the metal-type character of the band structure of the tubules. The high-energy shift of the σ states relative to the occupied π states is seen to be the most significant effect of the interlayer interaction in the armchair double-wall pair. The large shifts of optical gaps of the tubules due to formation of the DWNTs complicate the determination of the structure of DWNTs on the basis of optical data. On the other hand, the results obtained open the opportunity to classify experimental data on the DWNTs more specifically.

PACS number(s): 73.22.−f, 73.63.Fg

I. INTRODUCTION

The double-wall carbon nanotubes (DWNTs) can be considered as a limiting case between the single-wall carbon nanotubes (SWNTs) and multiwall carbon nanotubes (MWNTs). The DWNT consists of two concentric graphene cylinders with extremely strong covalent bonding of atoms within the individual graphitic sheets, but very weak van der Waals type interaction between them. The DWNTs are very important from theoretical and experimental standpoint. They are essential for electronic device applications, because DWNTs are the molecular analogues to coaxial cables. Thus, a metallic@semiconducting or semiconducting@metallic DWNT can be, respectively, a molecular conductive wire covered by an insulator or a molecular capacitor in a memory device.[1–3] It is believed that the double-shell carbon cylinders would exhibit enhanced field emission, mechanical, thermal, and filters properties when compared to SWNTs.[4]

The production and characterization of DWNTs attracted the attention of numerous scientists. The DWNTs have been produced by several techniques such as the arc discharge method,[5,6] the catalytic chemical vapor deposition method,[7] and a method utilizing fusion reactions of fullerenes in

SWNTs.[8,9] The DWNT yield can be greater than 95%.[10] The two constituent tubules of the DWNT can be characterized in detail by measuring the Raman spectra and high-resolution transmission electron microscopy.[11–13] Particularly, the indices of the two coaxial layers of a DWNT can be assigned based on the radial breathing mode frequencies, and the atomic correlations between two graphene layers in DWNT can be obtained using electron microscopy. In the DWNTs, the interlayer spacing is not a constant, ranging from 3.4 Å (the interlayer distance of graphite) to 4.1 Å.[12] Recently, the electronic structure of individual DWNTs suspended in water and in air over trenches was studied using optical absorption, emission, and time-resolved photoluminescence spectroscopy; it was shown experimentally that interaction of the two layers influences the optical transitions of the inner and outer tubules.[14,15]

Theoretical studies of the nanotube electronic structure perturbations due to interwall interaction in DWNTs have received much attention since 1993.[1] However, the full understanding of intertube transfer effects has not been achieved yet. The first calculation for a band structure of DWNT was done using the tight-binding π-electronic technique, which sensitively includes all symmetry constraints, but in a strongly simplified Hamiltonian.[1] It was shown that

the energy dispersion relations of SWNTs are weakly perturbed by the interlayer interaction. More specifically, the calculated energy band structures of the best matched commensurate[1] metallic@metallic armchair (5,5)@(10,10) and zigzag (9,0)@(18,0) nanotubes with the number of carbon atoms ratio in the layers equal to 1:2 yield a metallic DWNT when a weak interlayer coupling between the concentric nanotubes is introduced. The calculated coaxial incommensurate zigzag metallic@semiconducting (9,0)@(17,0) and semiconducting@metallic (10,0)@(18,0) nanotubes also retain their individual metallic and semiconducting identities when the weak interlayer interaction is turned on. Finally, two coaxial semiconducting zigzag tubules remain semiconducting when the weak interlayer coupling is introduced.

Closer examination of the interwall vibronic interaction effects was performed in the terms of tight-binding calculations with parametrization of the linear combination of atomic orbitals (LCAO) matrix elements based on *ab initio* results for simpler structures.[16,17] The electronic structure was calculated for three DWNTs in a Fermi level E_F region. For the (5,5)@(10,10) DWNT, it was predicted that the weak intertube interaction periodically opens and closes four pseudogaps in the density of states due to symmetry lowering during the low-frequency librational motion about and vibrational motion normal to the double-tube axis. As the intertube interaction is switched on in the (9,0)@(18,0) DWNT, the 30 meV gap opens.[17] In the semiconducting (8,0)@(17,0) system, the intertube interaction reduces the gap of the noninteracting system by 0.1 eV.[17] The band structure of the (5,5)@(10,10) DWNT obtained using a pseudopotential method and a plane-wave basis[18] resembles the tight-binding results.[17] Using a scattering technique based on a LCAO Hamiltonian, the ballistic quantum conductance of (10,10)@(15,15) finite nanotube was calculated.[19] It was found that the interwall interaction blocks certain conduction channels and redistributes the current nonuniformly across the walls providing an explanation for the unexpected integer and noninteger conductance values reported for multiwall nanotubes.[20]

Using the self-consistent plane-wave pseudopotential calculations, the work functions of the small-diameter DWNTs starting from the (4,0)@(13,0) and (3,3)@(8,8) nanotubes were studied.[21] In the case of DWNTs with ultrasmall inner tubules, the calculations show that the electrostatic interwall charge transfer induced effects result in the few tenth of eV (up to 0.5 eV) band shift due to the large (up to 1.25 eV) difference between the Fermi energies of the inner and outer tubules. It is very important for our work that these effects decrease drastically as one goes to the DWNTs with larger diameters. Particularly, in the largest zigzag (8,0)@(17,0) and armchair (5,5)@(10,10) DWNTs calculated,[21] the shifts are equal to 0.05 eV and 0.02 eV, respectively, that is negligible in comparison with the tunneling effects studied in our paper (see below). The charge transfer between the inner and outer tubules of the DWNTs with larger diameters is shown to be negligible, because the Fermi level energies are equal for the SWNTs with diameters larger than 1 nm.[21]

Finally, with due account of the cylindrical geometry of the nanotubes, a numerical technique for a local-density-functional calculation of the nanotubes electronic structure was presented and applied to DWNTs,[22] but for strongly oversimplified structural model of the nanotubes, where the point charges of the individual C^{4+} ions in the walls with graphitic honeycomb lattice were replaced by the two-dimensional infinitely thin structureless charged "sheets" of cylindrical symmetry with uniform surface-charge density.

A linear augmented cylindrical wave (LACW) method[23–25] is a more satisfying local-density-functional approach to determining the electronic states of nanotubes, in which one takes into account the cylindrical geometry of the nanotubes and considers a real approximately van der Waals width of the cylindrical layer and a real atomic structure of nanotubes. It is the aim of this work to study the perturbations of the electronic band structures and densities of states (DOS) of the core and shell tubes due to the intertube coupling in DWNTs in the terms of this method. For this purpose, we calculate the complete band structure of the purely semiconducting zigzag $(n,0)@(n',0)$ and purely metallic armchair $(n,n)@(n',n')$ DWNTs and use the results to correlate the minimum direct energy gaps E_{11} between the conduction and valence band singularities with the nanotubes diameters. It is to be noted that the latest optical absorption and time-resolved photoluminescence measurements of DWNTs have shown that one can determine experimentally the partial DOS and interband optical transition energies associated with core and shell tubes.[9,14]

Previously, the LACW method was successfully used to correlate the minimum direct energy gaps between the conduction and valence band singularities of metallic and semiconducting SWNTs with the nanotube structure and optical absorption spectra.[26,27] The effects of transition metal intercalation on the electronic properties of the carbon and boron-nitride nanotubes, as well as an influence of impurity atoms on the carbon and boron-nitride SWNTs band structure were studied using this approach too.[23–25,28,29] On the basis of LACW method, a simple model for the electronic structure of SWNTs embedded in a crystal matrix was developed and used to discuss the transport properties of devices with nanotubes encapsulated in a semiconductor crystal.[30]

The LACW method, as applied to the nanotubes, has advantage over the conventional LCAO and plane-wave pseudopotential methods. While low level LCAO calculations are relatively easy to do, improving the accuracy quickly becomes both technically demanding and computationally very expensive.[31] The main concern with approaches of the LCAO method is the transferability of the basis set; moreover, the LCAO basis is adequate to achieve good results for the valence band, but not for the conduction band, because this basis does not include the delocalized conducting plane-wave type functions. The plane-wave pseudopotential calculations suffer from a slow convergence and an unfavorable scaling: the number of basis functions and time taken to perform such a calculation on a computer increases asymptotically with the cube of the number of atoms.[31] This cubic scaling is a consequence of the purely delocalized nature of the plane-wave basis set. For example, in the case of the DWNTs, the single-electron wave functions were expanded in about 3×10^5 plane waves;[21] the LACW calculations of these systems require about 10^3 basis functions. One

way around slow convergence of the plane-wave pseudopotential method is a construction of the generalized Wannier functions by confining them to spherical regions centered on atoms as in a muffin-tin approach.[31] However, this version of pseudopotential methods has not been yet applied to the nanotubes. The basis of the LACW method has both localized and delocalized components. Finally, the main argument for using cylindrical waves is to account for the cylindrical geometry of the nanotubes in an explicit form that offers the obvious advantages.

II. THEORY

A. Electron potential

The LACW method is just a reformulation for cylindrical multiatomic systems of the linear augmented plane-wave (LAPW) theory.[32–34] In common with the standard and most simple LAPW technique for bulk materials,[32–34] in LACW method, a one-electron potential is used and the approximations are made in the sense of muffin-tin (MT) potentials and local density functional theory only. However, the electronic potential of a nanotube differs drastically from that of bulk material. Indeed, infinite motion of an electron is possible in any direction in a crystal, but it is obviously limited in the case of nanotubes by their size and shape. In terms of the LACW method, the atoms of DWNT are considered to be enclosed between two essentially impenetrable (in our model, infinite) cylinder-shaped potential barriers Ω_{b1} and Ω_{a2}, because there are two vacuum regions Ω_v on the outside of the tubule 2 and on the inside of the tubule 1 (Fig. 1). On the other hand, the cylinder-shaped potential barriers Ω_{a1} and Ω_{b2} on the outside of the tubule 1 and on the inside of the tubule 2 are penetrable (finite) ones, so that electron tunneling exchange between the tubules 1 and 2 is possible. The radii a_1, b_1 and a_2, b_2 of these barriers are chosen so that the regions confined by barriers accommodate a significant portion of the electron density of the tubules 1 and 2, respectively. Based on our previous calculations of the SWNTs, for zigzag nanotubes, we take $a_j = R_j + 2.3$ a.u., $b_j = R_j - 2.3$ a.u., and the cutoff energy $E_{cut} = 50$ eV (here, R_j is radius of the tubule j). For armchair nanotubes, we take $a_j = R_j + 2.4$ a.u., $b_j = R_j - 2.6$ a.u., and $E_{cut} = 100$ eV. This choice determines up to 600 basis functions for SWNTs and up to 1100 basis functions for DWNTs and permits a description of all the valence and the most important low-lying conduction band states, but not the nearly free electron states located about 2.3 Å away from the carbon layer (3 or 4 eV above E_F, 2 or 1 eV below vacuum).[35]

For simplicity, we treat the classically forbidden region Ω_f between barriers Ω_{a1} and Ω_{b2} as a homogenous medium with a constant classically impenetrable potential V_f. This potential is treated as a parameter. To characterize the barrier V_f, we used the dimensionless barrier parameter ϵ defined as $\epsilon = V_f/\delta$, where δ is energy gap between the Fermi level of the SWNTs and the interspherical potential.[30] All the results presented here are obtained for $\epsilon = 7$ determined with account of the graphite band structure. In graphite, the interlayer interactions introduce band splitting and shift of roughly 2−1 eV. For example, the three-dimensional graphite calcu-
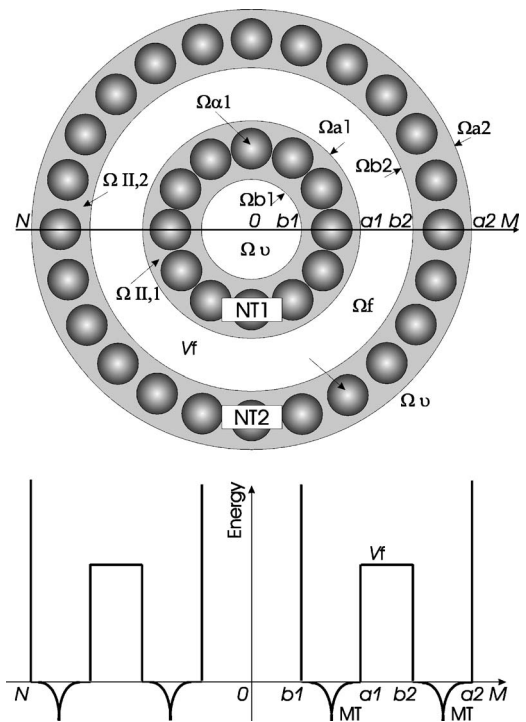
FIG. 1. DWNT (above) and cross section of the electronic potential along $N0M$ line (below). Here, NT_1 and NT_2 are the inner and outer tubes, respectively; $\Omega_{II,1}$ and $\Omega_{II,2}$ are the interstitial regions of these tubules; the Ω_{a1} and Ω_{a2} are the muffin-tin regions of the tubules 1 and 2, respectively; the Ω_{b1} and Ω_{a2} are the inner and outer impenetrable cylindrical potential barriers between the DWNT and vacuum regions Ω_v; V_f is a potential energy in Ω_f region between the finite cylindrical potential barriers Ω_{a1} and Ω_{b2}.

lations using the first principle muffin-tin and full-potential Korringa-Kohn-Rostoker technique suggest that the perturbations of valence π and σ bands are equal to 4−2 and 1−0.5 eV, respectively.[36] In DWNTs with the same interlayer separation, the band splitting and shift should be roughly less by half, because every graphene layer interacts with two neighbor layers in graphite, but there is only one interlayer coupling in the nanotube. Moreover, we would expect the interlayer interaction to decrease additionally for the nanotubes in comparison to graphite due to hybridization of π and σ states because of some curvature of the tubules. Therefore, in this paper, the potential V_f common for all DWNTs studied is chosen so that the average band splitting and shifts due to the intertube interaction are about 0.5 eV in the (5,5)@(10,10) DWNT; the (5,5) and (10,10) tubes show the graphitic interwall separation of 3.4 Å when nested.

Finally, the electronic potential is spherically symmetrical in the $\Omega_{I,1\alpha}$ and $\Omega_{I,2\alpha}$ regions of MT spheres α of atoms of tubules 1 and 2, respectively. Inside these spheres, we calculate the electron potential by means of the local density approximation with Slater exchange.[37–39] As usually, the radii of the MT spheres were chosen so that the atomic spheres touch, but do not overlap.

In the interatomic regions $\Omega_{II,1}$ and $\Omega_{II,2}$, the one-electron potential is constant; this constant potential is taken as the origin for measurements of energy.

In the LACW method, as different from the LAPW approach to bulk materials, the muffin-tin approximation requires an introduction of free parameters, namely, the width of cylindrical layer for the SWNTs and the constant potential V_f of the classically impenetrable region for the DWNTs. This complicates the self-consistent calculations of nanotubes in the terms of the LACW method. Both for the self-consistent and non-self-consistent calculations, the results depend on the choice of these parameters, the best fitted parameters being different in these cases. Particularly, our test self-consistent calculations of the SWNTs using a regular k-point mesh, where seven points were equally spaced between Brillouin zone center and boundary, show that the effect of self-consistency is virtually equivalent to that of a change of the width of cylindrical layer. Here, we perform the non-self-consistent calculations of the band structure of the DWNTs in order to avoid this ambiguity in the choice of parameter V_f, the electron density of the nanotubes being constructed as the superposition of the atomic ones. Surely, the non-self-consistent approach is more adequate for the systems without a significant change transfer. Therefore, we study the experimentally relevant semiconducting zigzag DWNTs with relatively large diameters starting from the (10,0)@(19,0) nanotube, as well as the metallic armchair (5,5)@(10,10) nanotube, for which the change transfer between the inner and outer tubules is negligible.[21] The band shifts and charge transfer effects are more pronounced in the small-diameter DWNTs, and the band structure results in these systems would be more sensitive both to the choice of the V_f and to the self-consistency corrections of the potential profile given in the Fig. 1. In order to improve the fixed potential and to perform the self-consistent LACW calculations of the nanotubes, one must develop a full-potential version of the model.

In the muffin-tin LACW approach, the electronic spectrum of the DWNTs is governed by the free movement of electron in the interatomic space of two cylindrical layers, by electron scattering on the MT spheres, and by electron tunneling through classically forbidden region Ω_f between the layers.

B. Basis functions

To construct the basis wave functions Ψ (linearized augmented cylindrical waves, LACWs) for DWNT, the solutions of the wave equation for the classically forbidden, interspherical, and MT regions of two tubules should be sewn together so that the resulting LACWs are continuous and differentiable anywhere in the system. In the interspherical region of the nanotubes and in the classically forbidden region between the tubules, the LACWs are the solutions of the Schrödinger equation for a free electron movement; in the cylindrical coordinates Z, R, Φ, this equation takes the form (in atomic Rydberg units)

$$\left[-\left(\frac{1}{R} \frac{\partial}{\partial R} R \frac{\partial}{\partial R} + \frac{1}{R^2} \frac{\partial^2}{\partial \Phi^2} + \frac{\partial^2}{\partial Z^2} \right) + U(R) \right] \Psi(Z, R, \Phi)$$
$$= E\Psi(Z, R, \Phi), \tag{1}$$

where

$$U(R) = \begin{cases} 0, & b_1 \leqslant R \leqslant a_1, \quad b_2 \leqslant R \leqslant a_2, \\ \infty, & R < b_1, R > a_2, \\ V_f, & a_1 \leqslant R \leqslant b_2. \end{cases} \tag{2}$$

Due to cylindrical symmetry of the potential $U(R)$, the solutions of Eq. (1) have the form $\Psi = \Psi_{PMN} = \Psi_P(Z)\Psi_M(\Phi)\Psi_{|M|N}(R)$, where

$$\Psi_P(Z, k) = \frac{1}{\sqrt{c}} \exp(iK_P Z), \quad K_P = k + k_P,$$

$$k_P = P(2\pi/c), \quad P = 0, \pm 1, \pm 2, \dots . \tag{3}$$

The function $\Psi_P(Z, k)$ corresponds to the movement of an electron along the Z axis in a one-dimensional system with periodic boundary conditions; c is a lattice constant for the Z direction; k is a one-dimensional crystal momentum, $-\pi/c \leqslant k \leqslant \pi/c$. The function

$$\Psi_M(\Phi) = \frac{1}{\sqrt{2\pi}} \exp(iM\Phi), \quad M = 0, \pm 1, \pm 2, \dots \tag{4}$$

corresponds to the rotation of an electron about the Z axis. The function $\Psi_{|M|N}(R)$ corresponds to the radial movement of an electron in the interspherical regions $\Omega_{II,j}$ ($j = 1, 2$) of the two tubules and in the classically forbidden region Ω_f; it is a solution of the equation

$$\left(-\frac{1}{R} \frac{d}{dR} R \frac{d}{dR} + \frac{M^2}{R^2} \right) \Psi_{|M|,N}(R) + U(R)\Psi_{|M|,N}(R)$$
$$= E_{|M|,N} \Psi_{|M|,N}(R). \tag{5}$$

Here, $E_{|M|,N}$ is the energy spectrum, and N is the radial quantum number. The energy

$$E = K_p^2 + E_{|M|,N} \tag{6}$$

corresponds to the wave function $\Psi_{PMN}(Z, R, \Phi)$.

In the regions $\Omega_{II,j}$, $U(R) = 0$ and Eq. (5) takes the form of the Bessel equation[40,41]

$$\left(\frac{d^2}{dR^2} + \frac{1}{R} \frac{d}{dR} + \kappa_{|M|,N}^2 - \frac{M^2}{R^2} \right) \Psi_{II,|M|,N}(R) = 0, \tag{7}$$

where $\kappa_{|M|,N} = (E_{|M|,N})^{1/2}$. Any solution of this equation is represented by a linear combination of cylindrical Bessel functions of the first J_M and second Y_M kinds,

$$\Psi_{II,|M|,N}(R) = C_{M,N}^{J,j} J_M(\kappa_{|M|,N}R) + C_{M,N}^{Y,j} Y_M(\kappa_{|M|,N}R), \quad j = 1, 2. \tag{8}$$

In the Ω_f region, $U(R) = V_f$ and $\Psi_{f,|M|,N}(R)$ must obey the equation

$$\left[\frac{d^2}{dR^2} + \frac{1}{R} \frac{d}{dR} - (V_f - \kappa_{|M|,N}^2) - \frac{M^2}{R^2} \right] \Psi_{f,|M|,N}(R) = 0. \tag{9}$$

We calculate the DWNT electron energy levels located below the potential V_f of the classically forbidden region. At $V_f > \kappa_{|M|,N}^2$, Eq. (9) is the modified Bessel equation.[40,41] Its solutions are the linear combinations of modified Bessel functions of the first K_M and second I_M kinds,

$$\Psi_{f|M|,N}(R) = C_{M,N}^K K_M(\kappa_{|M|,N}^f R) + C_{M,N}^I I_M(\kappa_{|M|,N}^f R), \quad (10)$$

where $\kappa_{|M|,N}^f = (V_f - \kappa_{|M|,N}^2)^{1/2}$.

The function $\Psi_{\text{II}f,|M|N}(R)$ should vanish at $R = b_1$ and $R = a_2$,

$$C_{M,N}^{J,1} J_M(\kappa_{|M|,N} b_1) + C_{M,N}^{Y,1} Y_M(\kappa_{|M|,N} b_1) = 0, \quad (11)$$

$$C_{M,N}^{J,2} J_M(\kappa_{|M|,N} a_2) + C_{M,N}^{Y,2} Y_M(\kappa_{|M|,N} a_2) = 0, \quad (12)$$

be continuous and differentiable at $R = a_1$ and $R = b_2$,

$$C_{M,N}^{J,1} J_M(\kappa_{|M|,N} a_1) + C_{M,N}^{Y,1} Y_M(\kappa_{|M|,N} a_1)$$
$$= C_{M,N}^K K_M(\kappa_{|M|,N}^f a_1) + C_{M,N}^I I_M(\kappa_{|M|,N}^f a_1), \quad (13)$$

$$C_{M,N}^{J,2} J_M(\kappa_{|M|,N} b_2) + C_{M,N}^{Y,2} Y_M(\kappa_{|M|,N} b_2)$$
$$= C_{M,N}^K K_M(\kappa_{|M|,N}^f b_2) + C_{M,N}^I I_M(\kappa_{|M|,N}^f b_2), \quad (14)$$

$$\kappa_{|M|,N}[C_{M,N}^{J,1} J_M'(\kappa_{|M|,N} a_1) + C_{M,N}^{Y,1} Y_M'(\kappa_{|M|,N} a_1)]$$
$$= \kappa_{|M|,N}^f[C_{M,N}^K K_M'(\kappa_{|M|,N}^f a_1) + C_{M,N}^I I_M'(\kappa_{|M|,N}^f a_1)], \quad (15)$$

$$\kappa_{|M|,N}[C_{M,N}^{J,2} J_M'(\kappa_{|M|,N} b_2) + C_{M,N}^{Y,2} Y_M'(\kappa_{|M|,N} b_2)]$$
$$= \kappa_{|M|,N}^f[C_{M,N}^K K_M'(\kappa_{|M|,N}^f b_2) + C_{M,N}^I I_M'(\kappa_{|M|,N}^f b_2)], \quad (16)$$

and be normalized

$$\int_{b_1}^{a_2} |\Psi_{\text{II}f,|M|,N}(R)|^2 R \, dR = 1. \quad (17)$$

From Eqs. (11)–(17) we obtain the coefficients $C_{M,N}^{J,j}$ and $C_{M,N}^{Y,j}$ ($j = 1, 2$), $C_{M,N}^K$, $C_{M,N}^I$, and $\kappa_{|M|,N}$.

Thus, in regions $\Omega_{\text{II},1}$, $\Omega_{\text{II},2}$, and Ω_f, the form of the basis function $\Psi_{\text{II}f,PMN}$ is finally determined. It is a cylindrical wave and

$$\hat{H} \Psi_{\text{II}f,PMN} = (K_p^2 + \kappa_{|M|,N}^2) \Psi_{\text{II}f,PMN}. \quad (18)$$

It is worth noting that, in the interspherical regions $\Omega_{\text{II},1}$ and $\Omega_{\text{II},2}$ of DWNT, the cylindrical wave $\Psi_{\text{II},PMN}(Z, \Phi, R)$ has the same analytical form of the linear combination of the functions J_M and Y_M (8) as in the case of an isolated SWNT;[23–25] only the equations for $\kappa_{|M|,N}$, $C_{M,N}^{J,j}$, and $C_{M,N}^{Y,j}$, as well as their numerical values change.

As in LAPW theory or in LACW model of SWNT, inside the MT sphere α of the tubule j in the local spherical coordinate system ρ, θ, φ, the LACW Ψ_{PMN} of the double tube is expanded in spherical harmonics $Y_{lm}(\theta, \varphi)$,

$$\Psi_{\text{I},j\alpha,PMN}(\rho, \theta, \varphi) = \infty \sum_{l=0,}^{\infty} \sum_{m=-l}^{l} [A_{lm,j\alpha} u_{l,j\alpha}(E_{l,j\alpha}, \rho)$$
$$+ B_{lm,j\alpha} \dot{u}_{l,j\alpha}(E_{l,j\alpha}, \rho)] Y_{lm}(\hat{\rho}). \quad (19)$$

Here, $u_{l,j\alpha}$ is the solution of the radial Schrödinger equation

$$\hat{H}_{\text{MT}} u_{l,j\alpha}(\rho) = E_{l,j\alpha} u_{l,j\alpha}(\rho) \quad (20)$$

for energy $E_{l,j\alpha}$, $\hat{\rho} = (\theta, \varphi)$, and $\dot{u}_{l,j\alpha}(E_{l,j\alpha}, \rho) = \partial u_{l,j\alpha}(E_{l,j\alpha}, \rho) / \partial E_{l,j\alpha}$. In Rydberg units, this equation takes the form

$$\frac{1}{\rho} \frac{\partial^2}{\partial \rho^2}(\rho u_{l,j\alpha}) + \left(E_{l,j\alpha} - V_{j\alpha}(\rho) - \frac{l(l+1)}{\rho^2}\right) u_{l,j\alpha} = 0. \quad (21)$$

Here, $V_{j\alpha}(\rho)$ is the local density spherically symmetric potential in the region of the MT sphere $j\alpha$. Coefficients $A_{lm,j\alpha}$ and $B_{lm,j\alpha}$ are selected so that both the LACW Ψ_{PMN} and its derivative have no discontinuities at the boundaries of the MT spheres. However, the analytical form of the cylindrical wave $\Psi_{\text{II},PMN}$ near the MT spheres of the nanotube remains unaltered in going from the SWNT to the DWNT. Therefore, the analytical expressions for coefficients $A_{lm,j\alpha}$ and $B_{lm,j\alpha}$ presented for the SWNT in Refs. 23–25 remain valid in the case of DWNT,

$$A_{lm,j\alpha} = r_{j\alpha}^2 D_{lm,j\alpha}^{PMN} a_{lm,j\alpha}^{PMN}(r_{j\alpha}), \quad (22)$$

$$B_{lm,j\alpha} = r_{j\alpha}^2 D_{lm,j\alpha}^{PMN} b_{lm,j\alpha}^{PMN}(r_{j\alpha}). \quad (23)$$

Here, $r_{j\alpha}$ is a radius of MT sphere of atom α of tubule j,

$$D_{lm,j\alpha}^{PMN} = \frac{1}{\sqrt{2c}} \left(\frac{(2l+1)[(l-|m|)!]}{[(l+|m|)!]}\right)^{1/2} (-1)^{[0.5(m+|m|+l)]} i^l$$
$$\times \exp[i(K_P Z_{j\alpha} + M\Phi_{j\alpha})]$$
$$\times (-1)^M [C_{M,N}^{J,j} J_{m-M}(\kappa_{|M|,N} R_{j\alpha})$$
$$+ C_{M,N}^{Y,j} Y_{m-M}(\kappa_{|M|,N} R_{j\alpha})], \quad (24)$$

$$a_{lm,j\alpha}^{PMN}(r_{j\alpha}) = I_{2,j\alpha}^{PMN}(r_{j\alpha}) \dot{u}_{l,j\alpha}(r_{j\alpha}) - I_{1,j\alpha}^{PMN}(r_{j\alpha}) \dot{u}_{l,j\alpha}'(r_{j\alpha}), \quad (25)$$

$$b_{lm,j\alpha}^{PMN}(r_{j\alpha}) = I_{1,j\alpha}^{PMN}(r_{j\alpha}) u_{l,j\alpha}'(r_{j\alpha}) - I_{2,j\alpha}^{PMN}(r_{j\alpha}) u_{l,j\alpha}(r_{j\alpha}). \quad (26)$$

Where $Z_{j\alpha}$, $\Phi_{j\alpha}$, and $R_{j\alpha}$ are cylindrical coordinates of the atom α of tubule j; $u_{l,j\alpha}' = \partial u_{l,j\alpha} / \partial \rho$ and $\dot{u}_{l,j\alpha}' = \partial \dot{u}_{l,j\alpha} / \partial \rho$ are radial derivatives of the $u_{l,j\alpha}$ and $\dot{u}_{l,j\alpha}$ functions; finally, I_1 and I_2 are integrals of the augmented Legendre polynomials $P_l^{|m|}$,

$$I_1 = 2 \int_0^{\pi/2} \exp[i(K_P r_{j\alpha} \cos \theta)] J_m(\kappa_{|M|,N} r_{j\alpha} \sin \theta) P_l^{|m|}$$
$$\times (\cos \theta) \sin \theta \, d\theta, \quad (27)$$

$$I_2 = 2 \int_0^{\pi/2} \exp[i(K_P r_{j\alpha} \cos \theta)][iK_P \cos \theta J_m(\kappa_{|M|,N} r_{j\alpha} \sin \theta)$$
$$+ (1/2)\kappa_{|M|,N} \sin \theta] \times [J_{m-1}(\kappa_{|M|,N} r_{j\alpha} \sin \theta)$$
$$- J_{m-1}(\kappa_{|M|,N} r_{j\alpha} \sin \theta)] P_l^{|m|}(\cos \theta) \sin \theta \, d\theta. \quad (28)$$

Thus, at $b_1 \le R \le a_1$ and $b_2 \le R \le a_2$, the LACWs Ψ_{MNP} of DWNT have the same analytical form as for the noninteracting SWNTs, whereas, in the Ω_f region of DWNT,

$$\Psi_{MNP}(Z,\Phi,R) = e^{i(k+k_P)Z}e^{iM\Phi}[C_{M,N}^K K_M(\kappa_{|M|,N}^f R)$$

$$+ C_{M,N}^I I_M(\kappa_{|M|,N}^f R)]. \tag{29}$$

C. Overlap integrals and Hamiltonian matrix elements

The integral $\langle \Psi_{P_2M_2N_2}|\Psi_{P_1M_1N_1}\rangle$ of the product of the LACWs $\Psi_{P_2M_2N_2}^*$ and $\Psi_{P_1M_1N_1}$ over the unit cell Ω is equal to the integral of the product of cylindrical waves $\Psi_{\mathrm{II},f,P_2M_2N_2}^*$ and $\Psi_{\mathrm{II},f,P_1M_1N_1}$ over the interspherical regions $\Omega_{\mathrm{II},1}$ and $\Omega_{\mathrm{II},2}$ and classically forbidden region Ω_f plus the sum of the integrals of the product of spherical parts of the LACWs $\Psi_{\mathrm{I},j\alpha,P_2M_2N_2}^*$ and $\Psi_{\mathrm{I},j\alpha,P_1M_1N_1}$ over the MT regions,

$$\int_\Omega \Psi_{P_2M_2N_2}^* \Psi_{P_1M_1N_1} dV$$

$$= \int_{\Omega_{\mathrm{II},1}+\Omega_{\mathrm{II},2}+\Omega_f} \Psi_{\mathrm{II},f,P_2M_2N_2}^* \Psi_{\mathrm{II},f,P_1M_1N_1} dV$$

$$+ \sum_{j=1,2}\sum_\alpha \int_{\Omega_{j\alpha}} \Psi_{\mathrm{I},j\alpha,P_2M_2N_2}^* \Psi_{\mathrm{I},j\alpha,P_1M_1N_1} dV. \tag{30}$$

The integral over $\Omega_{\mathrm{II},1}+\Omega_{\mathrm{II},2}+\Omega_f$ is equal to the integral over Ω minus the sum of the integrals over the MT regions. Due to the fact that the cylindrical waves as solutions of the Schrödinger equation (1) are orthonormalized, the integral over Ω is equal to the product of the δ functions. As a result, Eq. (30) takes the form

$$\langle \Psi_{P_2M_2N_2}|\Psi_{P_1M_1N_1}\rangle$$

$$= \delta_{P_2M_2N_2,P_1M_1N_1}$$

$$- \sum_{j=1,2}\sum_\alpha \int_{\Omega_{j\alpha}} \Psi_{\mathrm{II},P_2M_2N_2}^* \Psi_{\mathrm{II},P_1M_1N_1} dV$$

$$+ \sum_{j=1,2}\sum_\alpha \int_{\Omega_{j\alpha}} \Psi_{\mathrm{I},j\alpha,P_2M_2N_2}^* \Psi_{\mathrm{I},j\alpha,P_1M_1N_1} dV. \tag{31}$$

Inasmuch as both the cylindrical wave $\Psi_{\mathrm{II},PMN}$ and spherically symmetrical part $\Psi_{\mathrm{I},j\alpha,PMN}$ of LACW in the MT regions have the same form for DWNT and constituent tubules, the expression for overlap integrals obtained for the SWNT[23–25] can be readily rewritten for the DWNT,

$$\langle \Psi_{P_2M_2N_2}|\Psi_{P_1M_1N_1}\rangle = \delta_{P_2M_2N_2,P_1M_1N_1} - \frac{1}{c}(-1)^{M_2+M_1}\sum_{j=1,2}\sum_\alpha \exp\{i[(k_{P_1}-k_{P_2})Z_{j\alpha}+(M_1-M_2)\Phi_{j\alpha}]\}$$

$$\times \sum_{m=-\infty}^\infty [C_{M_2,N_2}^{J,j}J_{m-M_2}(\kappa_{|M_2|,N_2}R_{j\alpha}) + C_{M_2,N_2}^{Y,j}Y_{m-M_2}(\kappa_{|M_2|,N_2}R_{j\alpha})][C_{M_1,N_1}^{J,j}J_{m-M_1}(\kappa_{|M_1|,N_1}R_{j\alpha})$$

$$+ C_{M_1,N_1}^{Y,j}Y_{m-M_1}(\kappa_{|M_1|,N_1}R_{j\alpha})]\left(I_{3,j\alpha}^{P_2M_2N_2,P_1M_1N_1} - r_{j\alpha}^4 \sum_{l=|m|}^\infty \frac{(2l+1)[(l-|m|)!]}{2[(l+|m|)!]}S_{lm,j\alpha}^{P_2M_2N_2,P_1M_1N_1}(r_{j\alpha})\right), \tag{32}$$

where

$$I_3 = 2\int_0^{\pi/2}\int_0^{r_{j\alpha}} \cos[r(k_{P_1}-k_{P_2})\cos\theta]J_m(\kappa_{|M_2|,N_2}r\sin\theta)$$

$$\times J_m(\kappa_{|M_1|,N_1}r\sin\theta)\sin\theta r^2 d\theta dr,$$

$$S_{lm,j\alpha}(r_{j\alpha}) = (a_{lm,\alpha}^{P_2M_2N_2})^* a_{lm,\alpha}^{P_1M_1N_1} + N_{l,j\alpha}(b_{lm,\alpha}^{P_2M_2N_2})^* b_{lm,\alpha}^{P_1M_1N_1}, \tag{33}$$

$$N_{l,j\alpha} = \int_0^{r_{j\alpha}} (u_{l,j\alpha})^2 r^2 dr. \tag{34}$$

Analogously, for the Hamiltonian matrix elements of DWNT we have

$$\int_\Omega \Psi_{P_2M_2N_2}^* \hat{H}\Psi_{P_1M_1N_1} dV$$

$$= \int_{\Omega_{\mathrm{II},1}+\Omega_{\mathrm{II},2}+\Omega_f} \Psi_{\mathrm{II}f,P_2M_2N_2}^* \hat{H}\Psi_{\mathrm{II}f,P_1M_1N_1} dV$$

$$+ \sum_{j=1,2}\sum_\alpha \int_{\Omega_{j\alpha}} \Psi_{\mathrm{I},j\alpha,P_2M_2N_2}^* \hat{H}_{\mathrm{MT}}\Psi_{\mathrm{I},j\alpha,P_1M_1N_1} dV. \tag{35}$$

Again, the integral over $\Omega_{\mathrm{II},1}+\Omega_{\mathrm{II},2}+\Omega_f$ is equal to the integral over Ω minus the sum of the integrals over the MT regions. In Ω, cylindrical wave $\Psi_{\mathrm{II}f,PMN}$ is the solution of Schrödinger equation (1) with energy $K_p^2+\kappa_{|M|,N}^2$ (18). As a result, Eq. (35) takes the form

$$\langle \Psi_{P_2M_2N_2}|\hat{H}|\Psi_{P_1M_1N_1}\rangle = (K_{P_2}K_{P_1} + \kappa_{|M_2|,N_2}\kappa_{|M_1|,N_1})\delta_{P_2M_2N_2,P_1M_1N_1} - \sum_{j=1,2}\sum_{\alpha}\int_{\Omega_{j\alpha}}\Psi^*_{\text{II},P_2M_2N_2}(-\Delta)\Psi_{\text{II},P_1M_1N_1}dV$$

$$+ \sum_{j=1,2}\sum_{\alpha}\int_{\Omega_{j\alpha}}\Psi^*_{\text{I},j\alpha,P_2M_2N_2}\hat{H}_{\text{MT}}\Psi_{\text{I},j\alpha,P_1M_1N_1}dV. \tag{36}$$

In the MT regions, the functions $\Psi_{\text{II},PMN}$ and $\Psi_{\text{I},j\alpha,PMN}$ have the same analytical form in the case of double-tubule and noninteracting constituent tubules. Thus, the equation for Hamiltonian matrix elements of DWNT can be easily obtained from that of SWNT,[23–25]

$$\langle \Psi_{P_2M_2N_2}|\hat{H}|\Psi_{P_1M_1N_1}\rangle = (K_{P_2}K_{P_1} + \kappa_{|M_2|,N_2}\kappa_{|M_1|,N_1})\delta_{P_2M_2N_2,P_1M_1N_1} - \frac{1}{c}(-1)^{M_2+M_1}\sum_{j=1,2}\sum_{\alpha}\exp\{i[(k_{P_1}-k_{P_2})Z_{j\alpha}+(M_1-M_2)\Phi_{j\alpha}]\}$$

$$\times \sum_{m=-\infty}^{\infty}[C^{J,j}_{M_2,N_2}J_{m-M_2}(\kappa_{|M_2|,N_2}R_{j\alpha})+C^{Y,j}_{M_2,N_2}Y_{m-M_2}(\kappa_{|M_2|,N_2}R_{j\alpha})][C^{J,j}_{M_1,N_1}J_{m-M_1}(\kappa_{|M_1|,N_1}R_{j\alpha})$$

$$+ C^{Y,j}_{M_1,N_1}Y_{m-M_1}(\kappa_{|M_1|,N_1}R_{j\alpha})]\left(K_{P_2}K_{P_1}I^{P_2M_2N_2,P_1M_1N_1}_{3,j\alpha} + \kappa_{|M_2|,N_2}\kappa_{|M_1|,N_1}I'^{P_2M_2N_2,P_1M_1N_1}_{3,j\alpha} + m_4^2I^{P_2M_2N_2,P_1M_1N_1}_{4,j\alpha}\right.$$

$$\left.- r_{j\alpha}^4\sum_{l=|m|}^{\infty}\frac{(2l+1)[(l-|m|)!]}{2[(l+|m|)!]}[E_{l,j\alpha}S^{P_2M_2N_2,P_1M_1N_1}_{lm,j\alpha}(r_{j\alpha})+\gamma^{P_2M_2N_2,P_1M_1N_1}_{lm,j\alpha}(r_{j\alpha})]\right), \tag{37}$$

where

$$I'_3 = 2\int_0^{\pi/2}\int_0^{r_{j\alpha}}\cos[r(k_{P_1}-k_{P_2})\cos\theta]J'_m(\kappa_{|M_2|,N_2}r\sin\theta)$$

$$\times J'_m(\kappa_{|M_1|,N_1}r\sin\theta)\sin\theta r^2 d\theta dr, \tag{38}$$

$$I_4 = 2\int_0^{\pi/2}\int_0^{r_{j\alpha}}\cos[r(k_{P_1}-k_{P_2})\cos\theta]J_m(\kappa_{|M_2|,N_2}r\sin\theta)$$

$$\times J_m(\kappa_{|M_1|,N_1}r\sin\theta)(\sin\theta)^{-1}d\theta dr, \tag{39}$$

$$\gamma_{lm,j\alpha} = (I_2^*I_1 + I_1^*I_2)\cdot u_{l,j\alpha}u'_{l,\alpha} - I_2^*I_2\cdot u_{l,j\alpha}u_{l,j\alpha} - I_1^*I_1\cdot u'_{l,j\alpha}u'_{l,j\alpha}. \tag{40}$$

Finally, using the secular equation

$$\det\|\langle\Psi_{P_2M_2N_2}|\hat{H}|\Psi_{P_1M_1N_1}\rangle - E_n(k)\langle\Psi_{P_2M_2N_2}|\Psi_{P_1M_1N_1}\rangle\| = 0,$$

$$\sum_{P_1M_1N_1}[\langle\Psi_{P_2M_2N_2}|\hat{H}|\Psi_{P_1M_1N_1}\rangle$$

$$- E_n(k)\langle\Psi_{P_2M_2N_2}|\Psi_{P_1M_1N_1}\rangle]c_{nk,P_1M_1N_1} = 0, \tag{41}$$

we calculate the dispersion curves $E_n(k)$ of DWNT and corresponding electronic wave functions

$$\psi_{nk}(\mathbf{r}) = \sum_{PMN}c_{nk,PMN}\Psi_{PMN}(\mathbf{r}). \tag{42}$$

In order to better appreciate how the electronic structure of DWNT evolves from that of the two constituent tubules, for the eigenstate $\psi_{nk}(\mathbf{r})$, it is instructive to calculate the prob-abilities $w_{j,nk}$ and $w_{f,nk}$ that electron is located on the tubule j and in the classically forbidden region

$$w_{j,nk} = \sum_{PMN}|c_{nk,PMN}|^2$$

$$\times \frac{(C^{J,j}_{M,N})^2 + (C^{Y,j}_{M,N})^2}{\sum_{i=1,2}[(C^{J,i}_{M,N})^2 + (C^{Y,i}_{M,N})^2] + (C^I_{M,N})^2 + (C^K_{M,N})^2},$$

$$j = 1,2, \tag{43}$$

$$w_{f,nk} = \sum_{PMN}|c_{nk,PMN}|^2$$

$$\times \frac{(C^I_{M,N})^2 + (C^K_{M,N})^2}{\sum_{i=1,2}[(C^{J,i}_{M,N})^2 + (C^{Y,i}_{M,N})^2] + (C^I_{M,N})^2 + (C^K_{M,N})^2}. \tag{44}$$

In our case of high barrier V_f and weak interlayer coupling, the probabilities $w_{j,nk}$ are about 1 or 0 for different dispersion curves and virtually independent on momentum k. In all the DWNTs considered below, the probabilities $w_{j,nk}$ were either larger than 0.99, or smaller than 0.01. Therefore, the energy dispersion relations $E_{j,n}(k)$ of DWNT can be characterized by the number of tubule j, on which electron is basically located, and one can present two band structures for DWNT corresponding to states of the inner and outer tubules, the total band structure of the DWNT being just a superposition of band structures of the core and shell systems.

TABLE I. Minimum energy gaps of SWNTs.

SWNT	E_{11}, eV
(10,0)	0.31
(11,0)	0.32
(13,0)	0.83
(14,0)	0.56
(16,0)	0.89
(17,0)	0.50
(19,0)	0.80
(20,0)	0.46
(22,0)	0.75
(23,0)	0.35
(25,0)	0.70
(26,0)	0.41
(28,0)	0.66
(29,0)	0.38
(31,0)	0.62

III. RESULTS

We first consider the semiconducting zigzag DWNTs. Experimental data[42] and our previous band structure calculations of semiconducting zigzag SWNTs $(n,0)$ with the values of diameter d from 4 to 20 Å testify that the minimum direct energy difference $E_{11} = E[\Gamma_{c1}(\pi)] - E[\Gamma_{v1}(\pi)]$ between

TABLE II. Minimum energy gaps E_{11} of the core and shell nanotubes in DWNTs and the shifts of the gaps ΔE_{11} due to formation of DWNTs from pairs of SWNTs.

DWNT	E_{11}, eV		ΔE_{11}, eV	
	core	shell	core	shell
(10,0)@(19,0)	0.64	0.65	0.32	−0.15
(10,0)@(20,0)	0.63	0.53	0.32	0.07
(11,0)@(19,0)	0.71	0.65	0.39	−0.16
(11,0)@(20,0)	0.71	0.53	0.39	0.07
(13,0)@(22,0)	1.02	0.55	0.19	−0.19
(13,0)@(23,0)	1.02	0.50	0.19	0.15
(14,0)@(22,0)	0.70	0.56	0.14	−0.19
(14,0)@(23,0)	0.70	0.50	0.14	0.15
(16,0)@(25,0)	0.94	0.52	0.04	−0.18
(16,0)@(26,0)	0.93	0.48	0.04	0.07
(17,0)@(25,0)	0.45	0.52	−0.05	−0.18
(17,0)@(26,0)	0.45	0.48	−0.05	0.07
(19,0)@(28,0)	0.76	0.46	−0.05	−0.20
(19,0)@(29,0)	0.76	0.46	−0.05	0.07
(20,0)@(28,0)	0.42	0.46	−0.05	−0.20
(20,0)@(29,0)	0.42	0.46	−0.05	0.07
(22,0)@(31,0)	0.75	0.40	0.00	−0.22
(23,0)@(31,0)	0.40	0.40	0.06	−0.22
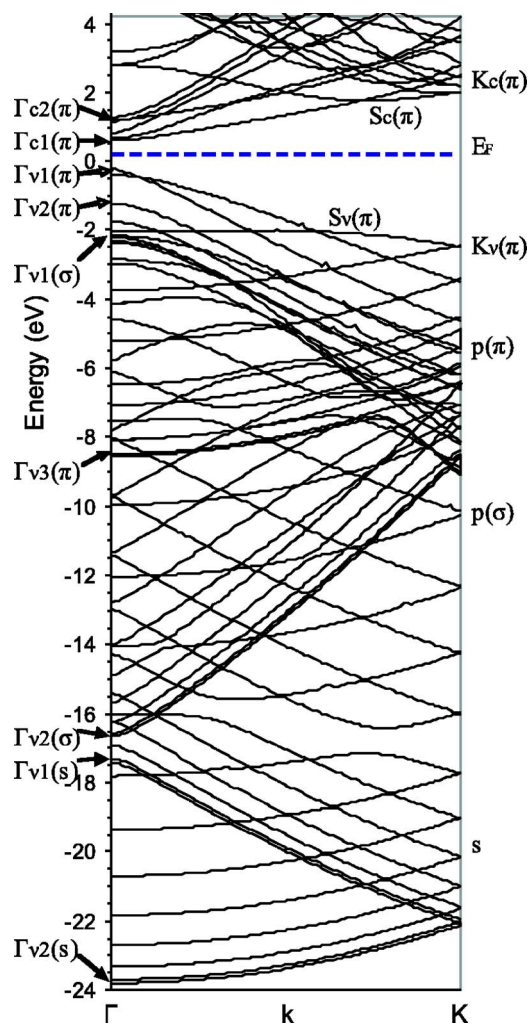
FIG. 2. (Color online) Band structure of (13,0) SWNT.

the singularities of the conduction and valence bands depend on whether dividing n by three leaves a remainder of 1 or 2 ($n \bmod 3 = 1$ or $n \bmod 3 = 2$). The gap energy $E_{11}(d^{-1})$ is oscillating function that gradually decays to zero as d^{-1} goes to zero, reaches a maximum at d^{-1} between 0.08 and 0.1 Å^{-1} ($13 \leqslant n \leqslant 16$), and decreases abruptly at $d^{-1} > 0.1$ Å^{-1} ($n \leqslant 11$). The curve $E_{11}(d^{-1})$ for $n \bmod 3 = 1$ is located totally above analogous curve for $n \bmod 3 = 2$. For zigzag SWNTs with about the same diameters, these gaps are approximately less by half for tubules with $n \bmod 3 = 2$ than for those with $n \bmod 3 = 1$. Thus, the $(n,0)$ SWNTs with $n \bmod 3 = 2$ and 2 can be thought of as the wide and low gap semiconductors, respectively (Table I). In the semiconducting zigzag SWNTs, the dependence of the E_{11} on whether $n \bmod 3 = 1$ or 2 is a result of then trigonal warping effects which shift the transition energies from the linear relation on d^{-1} in the high energy region if $n \bmod 3 = 1$ and in the low energy region if $n \bmod 3 = 2$.[42–45]

Here, we have calculated the complete band structures and densities of states in the Fermi level region of the 20 purely semiconducting DWNTs $(n,0)@(n',0)$ with $10 \leqslant n \leqslant 23$ and $19 \leqslant n' \leqslant 32$. We omit the metallic structures having n or n' evenly divisible by 3 and consider the DWNTs with interlayer distance 3.2 Å $\leqslant \Delta d \leqslant$ 3.7 Å.
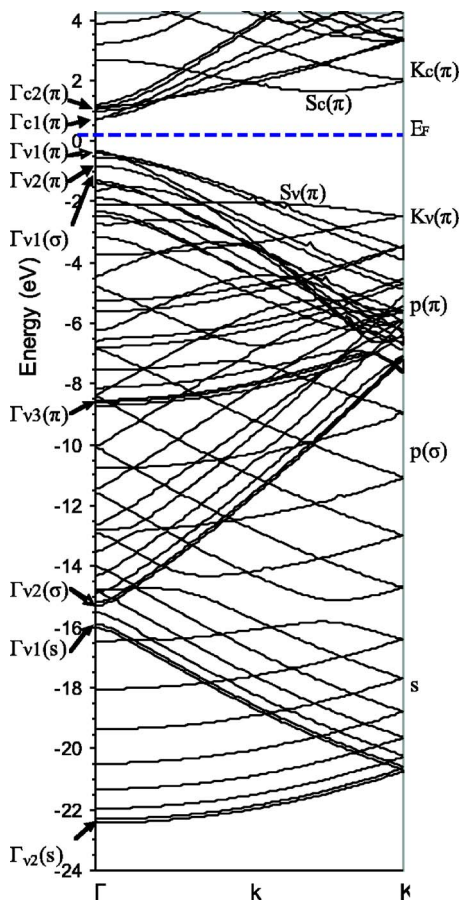
FIG. 3. (Color online) Band structure of core (13,0) tubule located inside (22,0) tubule.

FIG. 4. (Color online) Band structure of (22,0) SWNT.

Table II shows the minimum gaps E_{11} in the DWNTs and the shifts ΔE_{11} of these gaps due to the interwall perturbation. Figures 2–6 and Table III show representative results of the electronic structure calculations. The complete band structures and DOS in the Fermi level region of the SWNTs (13,0) and (22,0) can be compared with the analogous data for the core (13,0) and shell (22,0) tubules of the DWNT. In the DWNT (13,0)@(22,0), both inner and outer nanotubes belong to the $n \bmod 3 = 1$ series, the minimum energy gap (0.83 eV) of the small-diameter SWNT (13,0) being larger than that of the large-diameter SWNT (22,0) (0.76 eV) in agreement with simple approximate equation $E_{11} \sim d^{-1}$ known from π-electronic band structure calculations of the SWNTs. Our calculations indicate that the minimum gap E_{11} of (13,0) tube increases by 0.19 eV and that of (22,0) tube decreases by 0.19 eV due to formation of the DWNT, a significant value in device physics. The density of state curves in the Fermi level region show that there are analogous low energy shifts of the second gap $E_{22} = E[\Gamma_{c2}(\pi)] - E[\Gamma_{v2}(\pi)]$ equal to 0.3 and 0.4 eV in the case of (13,0) and (22,0) tubes, respectively. The interwall coupling results in a distinctly stronger perturbation of the band structure of inner tube as compared to that of outer one. The reason is that an additional space located between the Ω_{b2} and Ω_{a2} barriers that become accessible to electrons of the small-diameter (13,0) tube due to the formation of DWNT is about 2 times greater

in comparison with a new accessible region between the Ω_{b1} and Ω_{a1} barriers in the case of electrons of the large-diameter (22,0) tube. For example, as one goes to the DWNT, the total valence band width $E_v = E_F - E[\Gamma_{2v}(s)]$ of (13,0) tube decreases by 1.40 eV and that of (22,0) tube increases by 0.04 eV only.

In the DWNT (14,0)@(22,0), the inner tube belongs to the $n \bmod 3 = 2$ small gap series. Here, the gap of the inner SWNT (14,0) equal to 0.42 eV is smaller than that of the outer $n \bmod 3 = 1$ SWNT (22,0) in conflict with the $E_{11} \sim d^{-1}$ equation. As the intertube interaction is switched on, the gap of the inner tubule grows by 0.14 eV and that of the outer tubule decreases by 0.19 eV, the relative values of the gaps E_{11} of the tubules being reversed in the SWNTs and DWNT. For the core and shell nanotubes, the gap shifts ΔE_{11} induced by the intertube coupling are oppositely directed both in the (13, 0)@(22,0) and (14, 0)@(22,0) DWNTs. The ΔE_{11} values are positive and negative for the inner and outer tubules, respectively.

In the (13, 0)@(23,0) DWNT with the wide gap inner and low gap outer nanotubes, the gap shifts of the two tubules $\Delta E_{11} = 0.19$ and 0.15 eV are almost equal and have the same positive sign. This is also true for the (14, 0)@(23,0) DWNT, where both tubules belong to the low gap $n \bmod 3 = 2$ series; here, the $\Delta E_{11} = 0.14$ and 0.15 eV for the core and shell systems.

Table II shows that, independent on the type of core tubule, the gap E_{11} of the shell nanotube decreases by
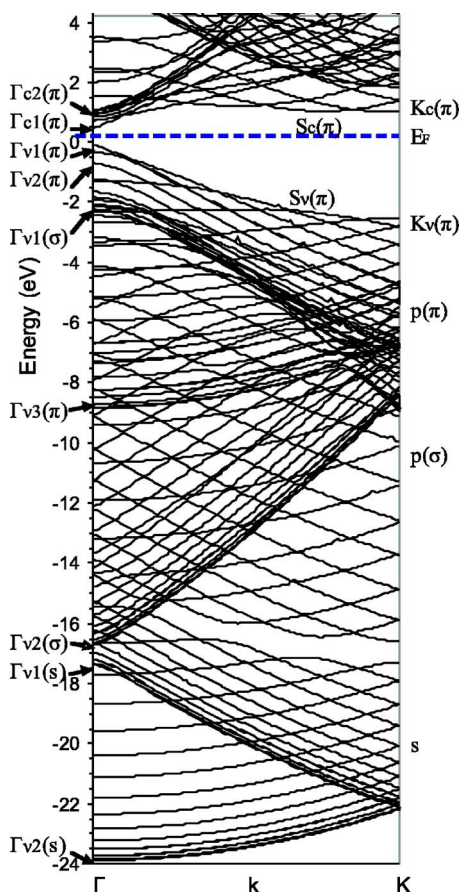
FIG. 5. (Color online) Band structure of outer (22,0) tubule interacting with inner (13,0) tubule.

0.15–0.22 eV, if this tube belongs to the n' mod $3=1$ series. On the other hand, for the shell tubes with n' mod $3=2$, the gap shift ΔE_{11} is always positive: $0.7 \leqslant \Delta E_{11} \leqslant 0.15$ eV. In both cases, the ΔE_{11} shifts do not decay, but slightly oscillate as one goes to the tubules with larger diameters d. For inner tubules, the ΔE_{11} shift depends strongly on the d. For n mod $3=2$ and n mod $3=2$ series with $10 \leqslant n \leqslant 16$, the shifts ΔE_{11} are positive, the maximum values of ΔE_{11} being equal to 0.32 and 0.39 eV, respectively. As one goes to the inner tubules with larger diameters, the shift ΔE_{11} quickly decays and thereupon varies between 0.06 and −0.05 eV.

Now let us consider the coaxial best matched metallic DWNT (5, 5)@(10,10) consisting of a D_{5d} (5,5) nanotube nested inside the D_{10h} (10,10) nanotube with the diameter ratio 1:2. In this most commensurate structure, there are two carbon atoms of the outer tubule for each carbon atom of the inner tubule; this geometry has many similarities to the *AB* stacking of graphite.[1] Figures 7 and 8 show all the occupied and unoccupied electronic states of SWNT (5,5) and the states of the core tubule (5,5) nested inside of the (10,10) tubule. The band structure of the (10,10) SWNT can be compared with that of the (10,10) outer tubule as the latter interacts with the inner (5,5) tubule (Figs. 9 and 10). Figure 11 shows influence of the interlayer interaction on the density of states of (5, 5)@(10,10) DWNT. The geometry was chosen to give rise to the most commensurate interlayer stacking, and the energy dispersion relations are seen to be strongly
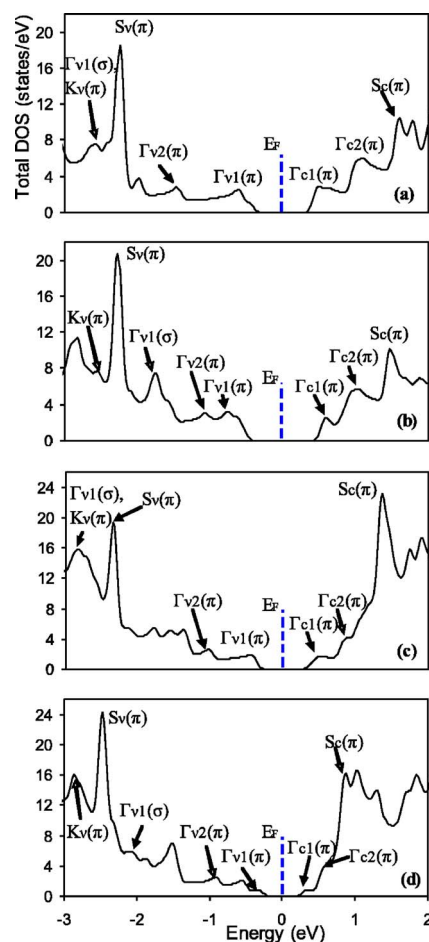
FIG. 6. (Color online) LACW DOS in the Fermi level region. Here and in Fig. 11, we use Gaussian broadening with a half-width of 0.05 eV. (a) (13,0) SWNT; (b) core (13,0) tubule nested in (22,0) tubule; (c) (22,0) SWNT; (d) shell (22,0) tubule with nested (13,0) tubule.

TABLE III. Energy levels of the (13,0) and (22,0) SWNTs and of these tubules in the (13,0)@(22,0) DWNT.

	Energy, eV			
Level	(13,0) SWNT	(13,0) core of DWNT	(22,0) SWNT	(22,0) shell of DWNT
$\Gamma_{c2}(\pi)$	0.95	0.79	0.81	0.53
$\Gamma_{c1}(\pi)$	0.41	0.51	0.37	0.29
$\Gamma_{v1}(\pi)$	−0.42	−0.50	−0.38	−0.28
$\Gamma_{v2}(\pi)$	−1.42	−0.75	−0.99	−0.89
$\Gamma_{v1}(\sigma)$	−2.35	−2.52	−2.53	−2.27
$\Gamma_{v3}(\pi)$	−8.74	−8.89	−8.79	−9.05
$\Gamma_{v2}(\sigma)$	−17.12	−15.48	−16.89	−16.88
$\Gamma_{v1}(s)$	−17.50	−16.10	−17.29	−17.19
$\Gamma_{v2}(s)$	−24.01	−22.63	−24.05	−24.10
$S_c(\pi)$	1.55	1.45	1.36	0.83
$S_v(\pi)$	−2.22	−2.25	−2.32	−2.43
$K_c(\pi)$	1.79	1.77	1.46	1.83
$K_v(\pi)$	−2.65	−2.67	−2.68	−2.74
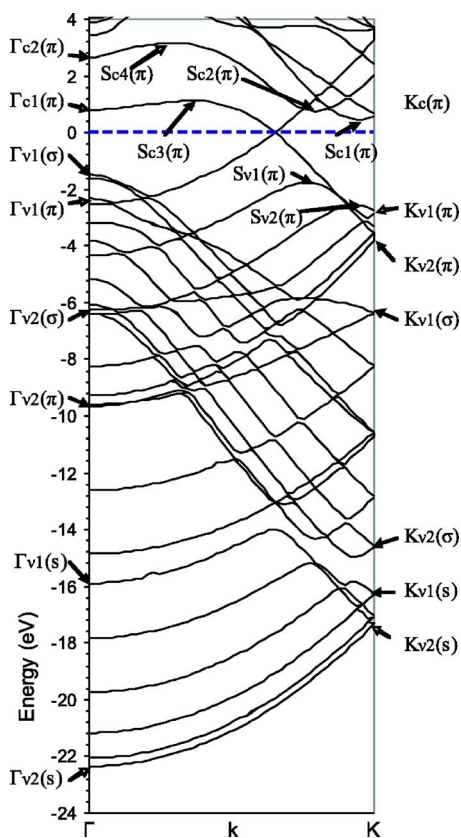
FIG. 7. (Color online) Band structure of (5,5) SWNT.
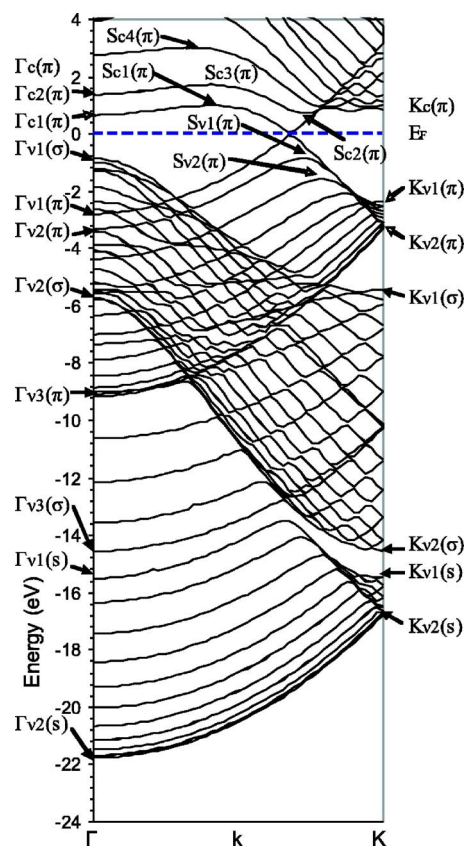
FIG. 9. (Color online) Band structure of (10,10) SWNT.
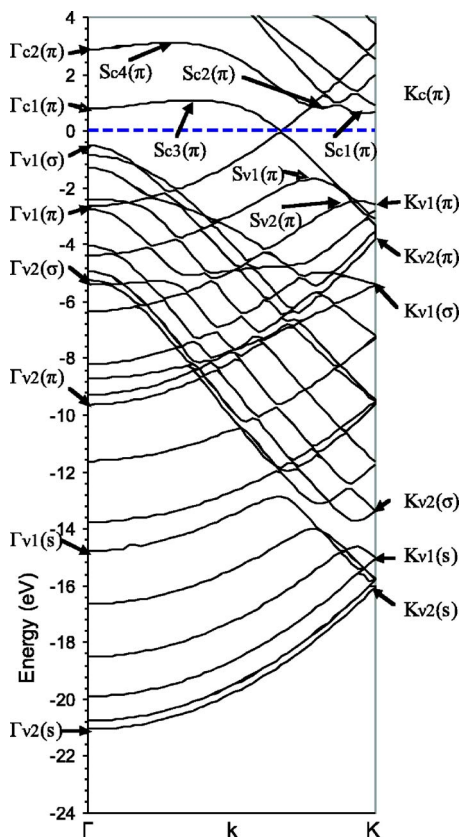
FIG. 8. (Color online) Band structure of the core (5,5) nanotube located inside (10,10) tubule.
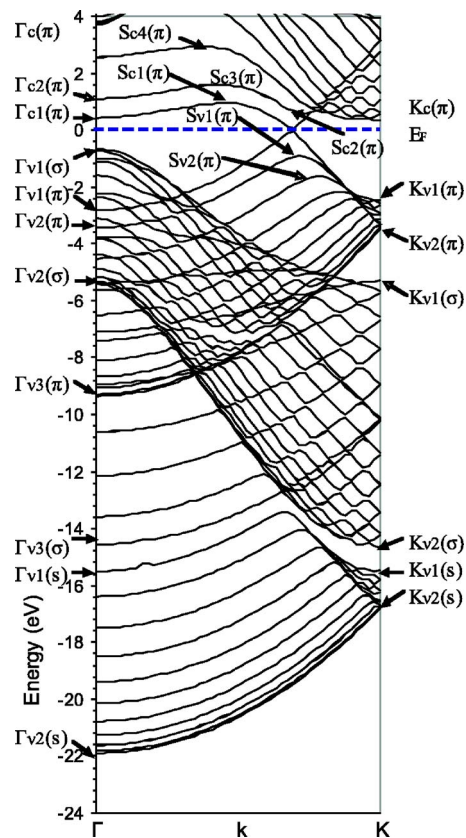
FIG. 10. (Color online) Band structure of the outer (10,10) interacting with inner (5,5) tubule.
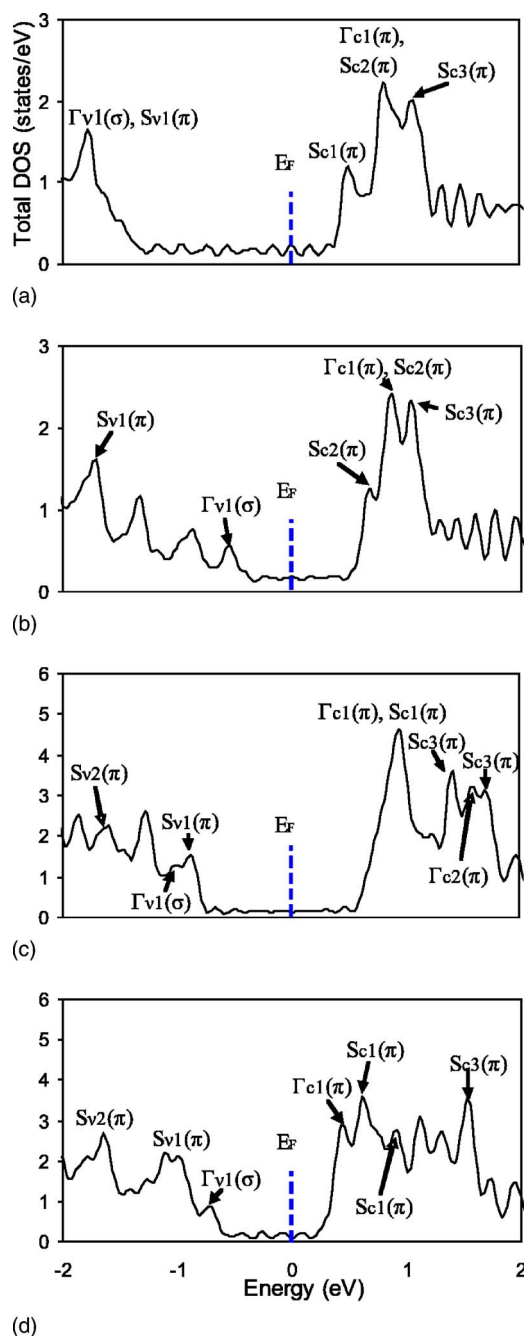
FIG. 11. (Color online) LACW DOSs in the Fermi level region. (a) (5,5) SWNT; (b) core (5,5) nested in (10,10) tube; (c) (10,10) SWNT; (d) shell (10,10) with nested (5,5) tube.

TABLE IV. Energy levels of the (5,5) and (10,10) SWNTs and of these tubules in the (5,5)@(10,10) DWNT.

Level	Energy, eV			
	(5,5) SWNT	(5,5) core of DWNT	(10,10) SWNT	(10,10) shell of DWNT
$\Gamma_{c2}(\pi)$	2.66	2.87	1.37	1.10
$\Gamma_{c1}(\pi)$	0.78	0.78	0.65	0.43
$\Gamma_{v1}(\sigma)$	−1.47	−0.51	−0.85	−0.67
$\Gamma_{v1}(\pi)$	−2.54	−2.66	−2.64	−2.82
$\Gamma_{v2}(\sigma)$	−6.38	−6.25	−5.72	−5.34
$\Gamma_{v2}(\pi)$	−9.59	−9.64	−9.17	−9.30
$\Gamma_{v1}(s)$	−15.89	−14.78	−15.49	−15.50
$\Gamma_{v2}(s)$	−22.35	−21.04	−21.75	−21.90
S_{c1}	0.76	0.83	0.48	0.48
S_{c2}	1.13	1.08	0.98	0.96
S_{c3}	3.16	3.10	1.73	1.59
S_{v1}	−1.76	−1.69	−0.84	−0.90
S_{v2}	−2.57	−2.48	−1.58	−1.64
$K_c(\pi)$	0.66	0.71	1.02	0.68
$K_v(\pi)$	−2.74	−2.59	−2.33	−2.45
$K_{v1}(\sigma)$	−6.34	−5.39	−5.44	−5.30
$K_{v2}(\sigma)$	−14.58	−13.35	−14.56	−14.65
K_s	−17.31	−16.01	−16.79	−16.75

occupied π states is seen to be the must significant effect of the interlayer interaction in the armchair double-wall pair.

This shift results in the significant perturbation of the most important direct optical σ-π^* and π-π^* transitions.

In the Brillouin zone center, the highest occupied σ state $\Gamma_{v1}(\sigma)$ is located above the highest occupied π state $\Gamma_{v1}(\pi)$ in all armchair SWNTs.[26] As the core tubule is nested in the shell tubule, the direct gap in the Γ point $E_{11}(\sigma, \pi^*)$ $=E[\Gamma_{c1}(\pi)]-E[\Gamma_{v1}(\sigma)]$ of the (5,5) and (10,10) tubules decreases by 0.96 and 0.40 eV, respectively. The energy gap $E_{11}(\pi, \pi^*)=E[S_{c1}(\pi^*)]-E[S_{v1}(\pi)]$ between the conduction and valence π-band singularities of the (5,5) tube increases and that of the (10,10) tubule decreses by 0.1 eV.

Formation of the (4, 4)@(9,9) DWNT results in the similar perturbation of the electronic structure of the core and shell tubules.

In conclusion, the large shifts of optical gaps of the tubules due to formation of the DWNTs complicate the determination of the structure of DWNTs on the basis of optical data. On the other hand, the results obtained open the opportunity to classify experimental data on the DWNTs more specifically.

perturbed by the interlayer coupling; however, the interlayer coupling does not break down the metal-type character of the band structures of the (5,5) and (10,10) tubules. The Fermi level is located at the intersection of the π bands at about $k=(2/3)(\pi/c)$ both in the SWNTs and in the double-walled pair. Formation of the DWNT (5, 5)@(10,10) results in increase of the valence band width E_v of the (5,5) tubule by 1.3 eV, the increase of the E_v of the (10,10) tubule being only 0.15 eV (Table IV); again, perturbation of the bands of core tubule is stronger in comparison with that of the shell tubule. A high-energy shift of the σ states relative to the

*Electronic address: dima@lester.ru

[1] R. Saito, G. Dresselhaus, and M. S. Dresselhaus, J. Appl. Phys. **73**, 494 (1993).

[2] G. Chen, S. Bandow, E. R. Margine, C. Nisoli, A. N. Kolmogorov, Vincent H. Crespi, R. Gupta, G. U. Sumanasekera, S. Iijima, and P. C. Eklund, Phys. Rev. Lett. **90**, 257403 (2003).

[3] A. N. Enyashin, G. Seifert, and A. L. Ivanovskii, JETP Lett. **80**, 608 (2004).

[4] Y. A. Kim, H. Muramatsu, T. Hayashi, M. Endo, M. Terrones, and M. S. Dresselhaus, Chem. Phys. Lett. **398**, 87 (2004).

[5] J. L. Hutchison, N. A. Kiselev, E. P. Krinichnaya, A. V. Krestinin, R. O. Loutfy, A. P. Morawsky, V. E. Muradyan, E. D. Obraztsova, J. Sloan, S. V. Terekhov, and D. N. Zakharov, Carbon **39**, 761 (2001).

[6] T. Sugai, H. Yoshida, T. Shimada, T. Okazaki, H. Shinohara, and S. Bandow, Nano Lett. **3**, 769 (2003).

[7] R. R. Bacsa, E. Flahaut, Ch. Laurent, A. Peigney, S. Aloni, P. Puech, and W. S. Bacsa, New J. Phys. **5**, 131 (2003).

[8] S. Bandow, M. Takizawa, K. Hirahara, M. Yudasaka, and S. Iijima, Chem. Phys. Lett. **337**, 48 (2001).

[9] S. Bandow, K. Hirahara, T. Hiraoka, G. Chen, and P. C. Eklund, MRS Bull. **29**, 260 (2004).

[10] M. Endo, H. Muramatsu, T. Hayashi, Y. A. Kim, M. Terrones, and M. S. Dresselhaus, Nature (London) **433**, 476 (2005).

[11] W. C. Ren, F. Li, J. Chen, S. Bai, and H. M. Cheng, Chem. Phys. Lett. **359**, 196 (2002).

[12] F. Li, S. G. Chou, W. Ren, J. A. Gardecki, A. K. Swan, B. B. Goldberg, and M. S. Dresselhaus, J. Mater. Res. **18**, 1251 (2003).

[13] A. Hashimoto, K. Suenaga, K. Urita, T. Shimada, T. Sugai, S. Bandow, H. Shinohara, and S. Iijima, Phys. Rev. Lett. **94**, 045504 (2005).

[14] T. Hertel, A. Hagen, V. Talalaev, K. Arnold, F. Hennrich, M. Kappes, S. Rosenthal, and J. McBride, Nano Lett. **5**, 511 (2005).

[15] Y. Yin, S. B. Cronin, A. G. Walsh, A. Stolyarov, M. Tinkham, A. N. Vamivakas, R. R. Bacsa, M. S. Unlu, B.B. Goldberg, A. Swan, and W. Bacsa, *Proceedings of the Nanotechnology Conference and Trade Show*, Anaheim, California (2005).

[16] Ph. Lambin, L. Philippe, J. C. Charlier, and J. P. Michenaud, Comput. Mater. Sci. **2**, 350 (1994).

[17] Y.-K. Kwon and D. Tomanek, Phys. Rev. B **58**, R16001 (1998).

[18] Y. Miyamoto, S. Saito, and D. Tomanek, Phys. Rev. B **65**, 041402(R) (2001).

[19] S. Sanvito, Y.-K. Kwon, D. Tomanek, and C. J. Lambert, Phys. Rev. Lett. **84**, 1974 (2000).

[20] S. Frank, P. Poncharal, Z. L. Wang, and W. A. de Heer, Science **280**, 1744 (1998).

[21] B. Shan and K. Cho, Phys. Rev. B **73**, 081401(R) (2006).

[22] D. Östling, D. Tomanek, and A. Rosèn, Phys. Rev. B **55**, 13980 (1997).

[23] P. N. D'yachkov, O. M. Kepp, and A. V. Nikolaev, Dokl. Chem. **365**, 67 (1999); in *Science and Application of Nanotubes*, edited by D. Tomanek and R. J. Enbody (Kluwer Academic/Plenum, New York, 2000), p. 77.

[24] P. N. D'yachkov and D. V. Kirin, Dokl. Phys. Chem. **369**, 326 (1999); in *Proceedings of the School and Workshop Nanotubes and Nanostructures*, edited by S. Bellucci [Ital. Phys. Soc., Conf. Proc. 74, 203 (2000)].

[25] P. N. D'yachkov, in *Encyclopedia of Nanoscience and Nanotechnology*, edited by H. S. Nalwa (American Scientific, San Diego, 2004), Vol. 1, p. 191.

[26] P. N. D'yachkov, H. Hermann, and D. V. Kirin, Appl. Phys. Lett. **81**, 5228 (2002).

[27] P. N. D'yachkov and H. Hermann, J. Appl. Phys. **95**, 399 (2004).

[28] A. V. Nikulkina and P. N. D'yachkov, Russ. J. Inorg. Chem. **49**, 430 (2004).

[29] A. Yu. Golovacheva and P. N. D'yachkov, JETP Lett. **82**, 834 (2005).

[30] P. N. D'yachkov and D. V. Makaev, Phys. Rev. B **71**, 081101(R) (2005).

[31] C.-K. Skylaris, P. D. Haynes, A. Mostofi, and M. C. Payne, J. Chem. Phys. **122**, 084119 (2005).

[32] O. K. Andersen, Phys. Rev. B **12**, 3060 (1975).

[33] D. D. Koelling and G. O. Arbman, J. Phys. F: Met. Phys. **5**, 2041 (1975).

[34] D. J. Singh, *Planewaves, Pseudopotentials and the LAPW Method* (Kluwer, Boston, 1994).

[35] S. Okada, A. Oshiyama, and S. Saito, Phys. Rev. B **62**, 7634 (2000).

[36] R. C. Tatar and S. Rabii, Phys. Rev. B **25**, 4126 (1982).

[37] J. C. Slater, *Quantum Chemistry of Molecules and Crystals*, vol. 4: The self-consistent field for molecules and solids (McGraw-Hill, New York, 1974).

[38] P. Hohenberg and W. Kohn, Phys. Rev. **136**, B864 (1964).

[39] W. Kohn and L. J. Sham, Phys. Rev. **140**, A1133 (1965).

[40] G. N. Watson, *Treatise on the Theory of Bessel Functions*, 2nd ed. (Cambridge University Press, New York, 1966).

[41] G. A. Korn and T. M. Korn, *Mathematical Handbook for Scientists and Engineers* (McGraw-Hill, New York, 1961).

[42] S. M. Bachilo, M. S. Strano, C. Kittrell, R. H. Hauge, R. E. Smalley, and R. B. Weisman, Science **298**, 2361 (2002).

[43] R. Saito, G. Dresselhaus, and M. S. Dresselhaus, Phys. Rev. B **61**, 2981 (2000).

[44] S. Reich, C. Thomsen, and P. Ordejon, Phys. Rev. B **65**, 155411 (2002).

[45] S. Reich, C. Thomsen, and J. Robertson, Phys. Rev. Lett. **95**, 077402 (2005).